

Supporting Information

Selective Formation of Linear Alkanes from *n*-Hexadecane Primary Hydrocracking in Shape-Selective MFI Zeolites by Competitive Adsorption of Water

Roald Brosius*, Patricia J. Kooyman, and Jack C. Q. Fletcher

Institute for Catalysis Research, Department of Chemical Engineering, University of Cape Town, Rondebosch 7701, South Africa

roald.brosius@uct.ac.za

Zeolite nanosheet synthesis

The structure directing agents (SDA) for NS synthesis were di-quaternary ammonium surfactant $[\text{C}_{22}\text{H}_{45}-\text{N}^+(\text{CH}_3)_2-\text{C}_6\text{H}_{12}-\text{N}^+(\text{CH}_3)_2-\text{C}_6\text{H}_{13}]$ and tetra-quaternary ammonium surfactant $[\text{C}_{22}\text{H}_{45}-\text{N}^+(\text{CH}_3)_2-(\text{C}_6\text{H}_{12}-\text{N}^+(\text{CH}_3)_2)_3-\text{C}_6\text{H}_{13}]$. The bromide forms of the SDAs were prepared via alkylation of tertiary amines by alkyl halides according to Choi et al.¹ The zeolite preparation method was adopted from Machoke et al.² and modified to allow for secondary nucleation assisted hydrothermal crystallization.³ Zeolite synthesis gels of composition 1 Al_2O_3 : 100 SiO_2 : a $\text{SDA}(\text{Br})_x$: 21 H_2SO_4 : 30 Na_2O : 4000 H_2O : 400 EtOH were prepared, where a was 10 using the di-quaternary SDA ($x = 2$) and 5 using the tetra-quaternary SDA ($x = 4$). For a preparation of 3 g of NS, first a seeding solution was prepared by dissolving 1.2 g NaOH (Sigma-Aldrich) in 27.3 g H_2O (1.1 M, pH 14.04), then adding 0.15 g H-MFI-90 and stirring this suspension in a 500 ml polypropylene bottle at 60 °C for 12 h resulting in a colloidal suspension of slightly blueish appearance. After cooling to room temperature, the SDA was dissolved under vigorous stirring (500 rpm) for 2 hours. Into this opaque soapy solution, a solution containing H_2SO_4 (Kimix 98.08 %, 0.3332 g), $\text{Al}_2(\text{SO}_4)_3 \cdot 18\text{H}_2\text{O}$ (Riedel de Haën, 0.882 g) and the remaining H_2O (8.35 g) were added dropwise during 20 min (1 drop every 5 sec). Exactly 40 min later, tetraethylorthosilicate (TEOS, Sigma-Aldrich, 9.896 g) is added at once under vigorous stirring. After 3 hours a somewhat viscous pourable hydrogel is used to fill 4 teflon lined stainless steel autoclaves (21 ml) to precisely 67 % of the available volume. The autoclaves are rotated at 60 rpm while the oven heats to 150 °C (5 °C/min) where hydrothermal crystallization occurs during 2.5 days. Samples were filtered, washed with water (H_2O 10 $\text{M}\Omega \cdot \text{cm}$ @ 25 °C) using 6 bar of compressed air in a pressure filtration unit, dried at 120 °C overnight and subsequently calcined in static air at 550 °C (heating rate 1 °C/min) for 8 hours. Calcined samples were ion-exchanged at room temperature with 500 ml of a 1 M NH_4Cl solution for 3 g of dry sample. Ion-exchange is repeated once and care is taken to rinse all Cl^- , this takes at least 10 l of water and another 5 l washing is done to be certain and the sample is dried overnight. The sample is calcined in static air again at 550 °C (heating rate 3 °C/min) for 1 hour. Each nanosheet sample in this study was prepared a minimum of three times to demonstrate reproducibility.

X-ray diffraction

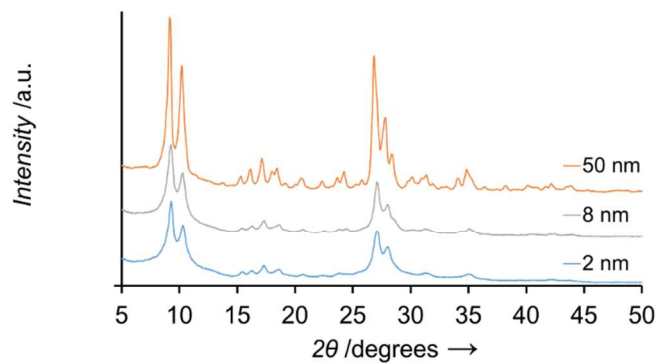


Figure S1. XRD of MFI, NS-8, NS-2 with 50 nm, 8 nm, and 2 nm sized crystalline domains respectively.

Transmission electron microscopy

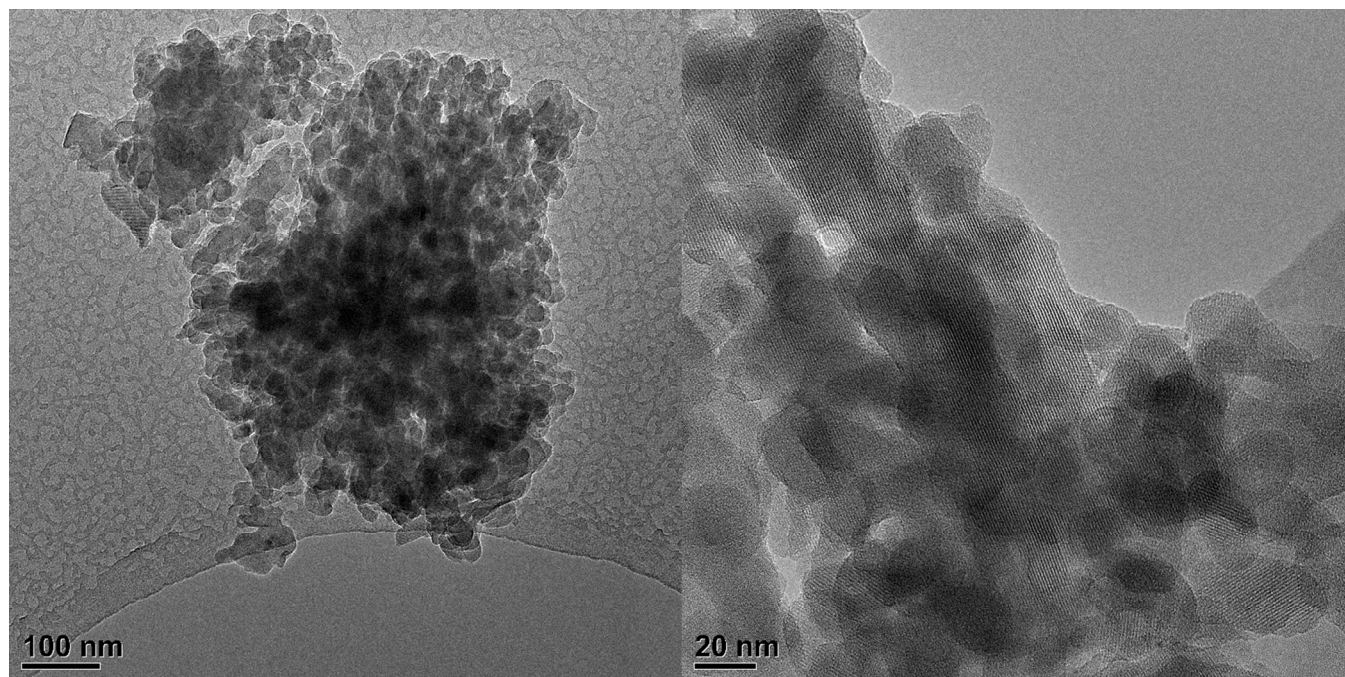


Figure S2. TEM images of zeolite MFI after calcination. Representative overview (left); detail (right).

N₂ adsorption

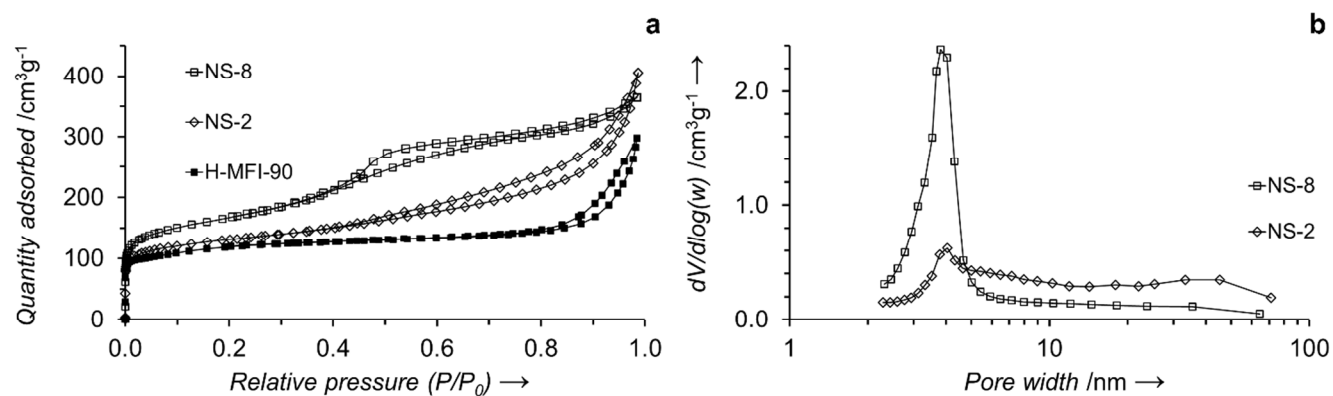


Figure S3. Textural characterization of zeolite MFI, NS-2 and NS-8. a) N_2 adsorption and desorption isotherms from MFI, NS-2 and NS-8; b) BJH pore size distribution plot calculated from the desorption branch of a) for NS-2 and NS-8.

Transmission electron microscopy

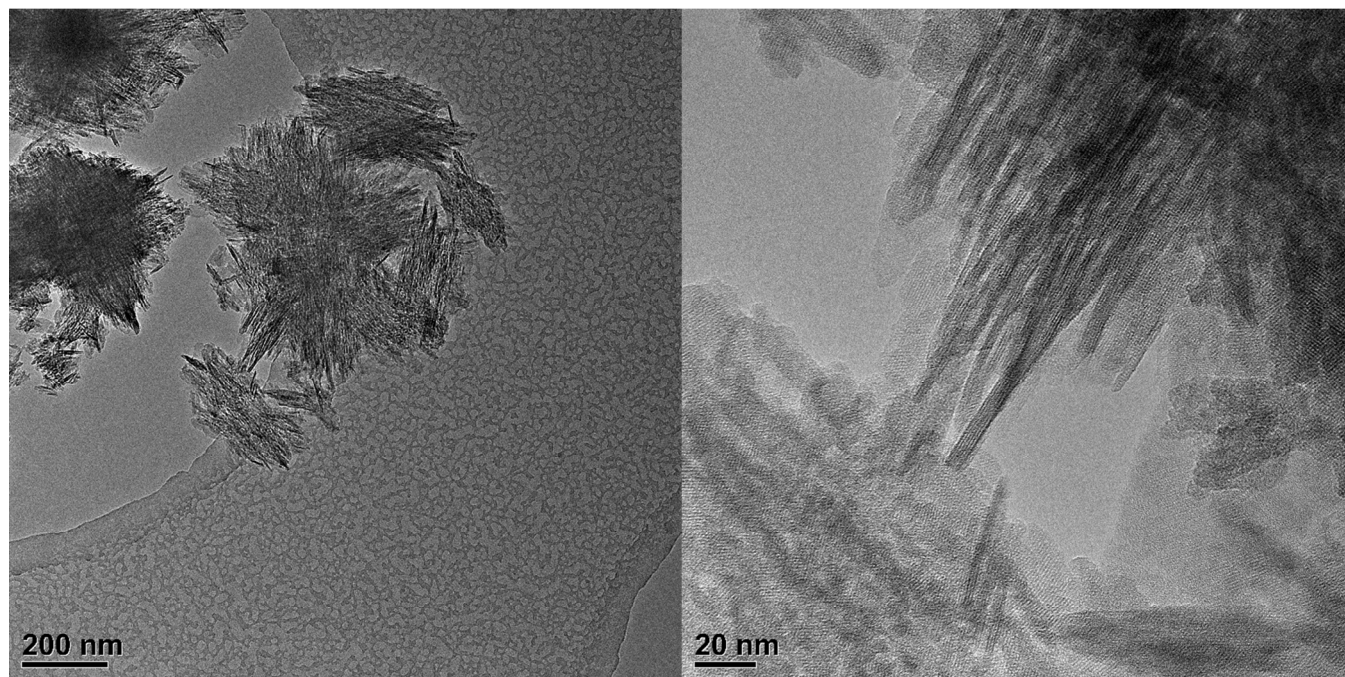


Figure S4. TEM images of zeolite nanosheet NS-2 after calcination. Representative overview (left); detail (right).

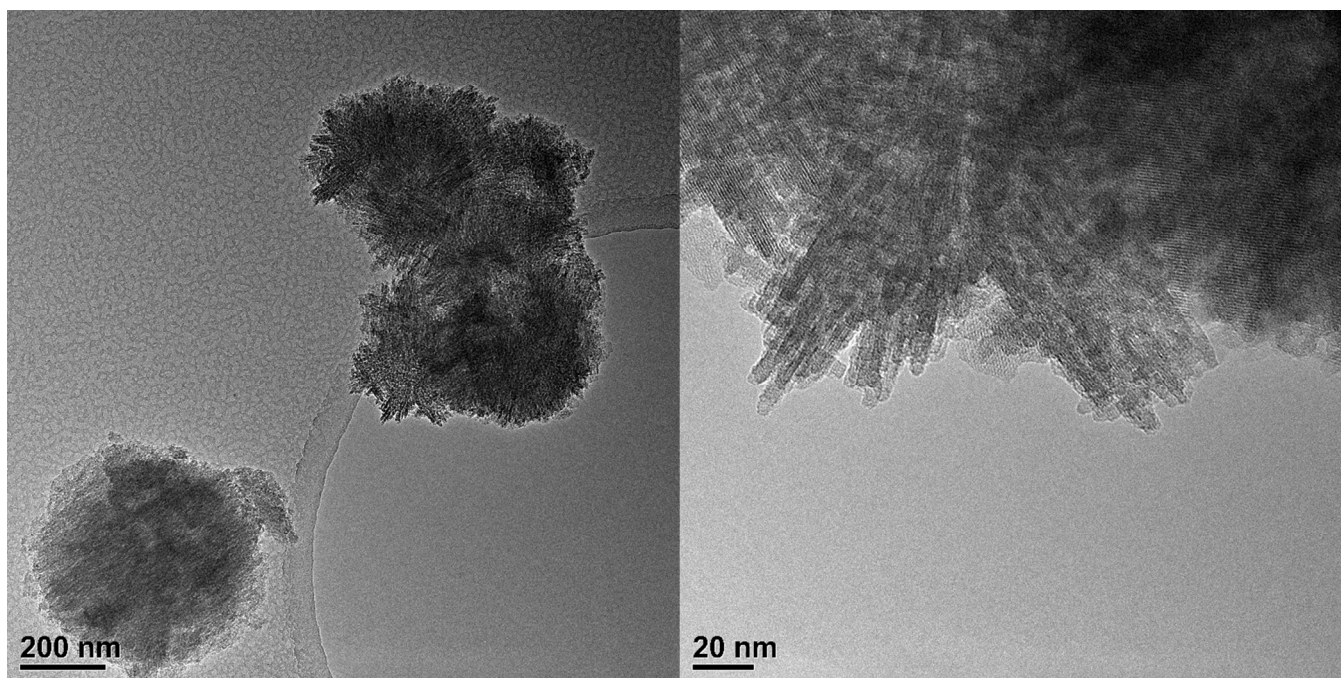


Figure S5. TEM images of zeolite nanosheet NS-8 after calcination. Representative overview (left); detail (right).

NH₃ temperature programmed desorption

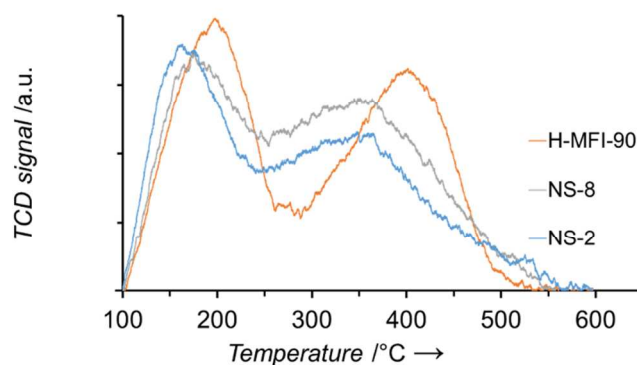


Figure S6. NH₃-TPD of H-MFI-90, H-NS-8 and H-NS-2.

CO chemisorption

A Pt/H-MFI sample of 0.3 g was subjected to the high (1 °C/min) and the low (0.3 °C/min, 0.4 °C/min) heating rate pretreatment – just as it is pretreated ahead of catalytic testing – in-situ prior to CO chemisorption at 35 °C, in a MicroMeritics ASAP2020 instrument. The dispersion γ (%) of the noble metal is calculated from [Eq. (1)];

$$\gamma (\%) = \frac{V_m/V_{mol}}{M\%/W_a} \cdot 100 \cdot 100 \quad (1)$$

with V_m is the volume of active gas chemisorbed (cm^3g^{-1} STP) determined at the monolayer, V_{mol} the molar volume of the adsorptive ($\text{cm}^3\text{mol}^{-1}$ STP), F_s the stoichiometry factor taken as 1 for CO adsorption on Pt, W_a the atomic weight of the metal (Pt: 195.08 gmol^{-1}) and $M\%$ the percentage of active metal by weight as grams of metal per gram of sample. The active particle size is calculated from [Eq. (2)];

$$d = \frac{6}{A_{Sm}\gamma\rho} \cdot 100 \quad (2)$$

with A_{Sm} representing the active area per gram of pure metal – calculated from the number of adsorptive molecules in the volume at the monolayer and the cross-sectional area of CO: $7.87 \cdot 10^{-2} \text{ nm}^2$ – ρ the density of the metal (Pt: 21.45 gcm^{-3}) and γ the dispersion in %. The dry sample weight is determined at the end of the chemisorption measurement. An example for Pt-1/MFI is shown in Figure S7, the monolayer volume is found on the Y-axis at the intercept of $1.0 \text{ cm}^3\text{g}^{-1}$, corresponding to a dispersion of 96.7 % and an average particle size of 1.2 nm. CO chemisorption was repeated twice to ascertain reproducibility.

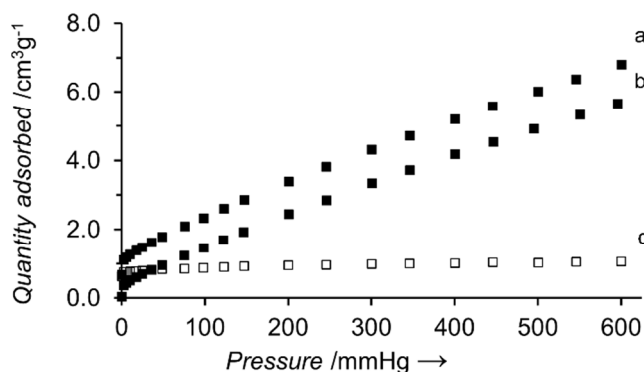


Figure S7. CO chemisorption on Pt-1/MFI oxidized at $0.3 \text{ }^\circ\text{Cmin}^{-1}$ to $350 \text{ }^\circ\text{C}$ and reduced at $0.4 \text{ }^\circ\text{Cmin}^{-1}$ to $225 \text{ }^\circ\text{C}$: a) chemisorption + physisorption, b) physisorption and c) difference of both.

Catalyst testing in an ideal plug flow reactor

The experimental laboratory reactor construction consist of the following parts in the order as they appear along the hydrodynamic flow: a vertically positioned $\frac{3}{4}$ " stainless steel tube reactor (16 mm ID), SiC filled vaporizer, dilution gas entry point, T-junction to sample line exit point with needle throttle valve, back-pressure regulator maintaining all of the above at a pressure of 20 bar. The reactor effluent, which is partly liquid and partly vapor, flows into the top of the evaporator where it spreads

over the SiC packing 5 cm above the point where dilution gas enters through a dip-tube. Between the reactor and the vaporizer the effluent cools down to 175 °C. A constant flow of N₂ dilution is fed to the vaporizer, where it brings about partial evaporation of the reactor effluent. Full evaporation is achieved gradually, along the length of the evaporator, due to the temperature gradient of approximately 1.5 °C/cm from 175 °C to 235 °C, before a needle valve at the bottom of the evaporator releases a small stream of the diluted now fully gaseous effluent to an online gas chromatograph (GC). The bulk of the diluted effluent passes through the back pressure regulator to the vent. In this manner, the standard deviation of the peak area of *n*-hexadecane in a large sample of GC injections (with a frequency of 1 every 30 min) during a 24h blank run (no catalyst) with *n*-hexadecane (0.03 sccm/min), H₂ (50 sccm/min) and N₂ dilution (250 sccm/min) was less than 1 % of the average.

Following catalyst pretreatment, the reactor was pressurized and H₂ and n-C₁₆ flow commenced at 225 °C. Steady state was reached after 24 hours on stream. Each of 4 parallel reactors was sampled at least 3 times spanning 12 h TOS at steady state before either temperature or space velocity was changed. To gain a statistically representative sample of the product distribution, the reaction conditions were changed on a daily basis and experiments ran for up to 14 days. Pt loaded zeolites catalysts were tested from 225 °C to 185 °C by down stepping the temperature and before introduction of water the temperature was returned to 225 °C. In the presence of water the temperature was gradually increased from 225 °C to 265 °C. No appreciable catalyst deactivation was observed during hydrocracking either with or without water.

Conversion of *n*-hexadecane, X(*n*-C₁₆), and product selectivities, S(C_{*i*}) are defined by [Eqs. (3), (4)]. *F_i* indicates the molar flow, *S* is the carbon selectivity toward a product with *n* carbon atoms. Peak areas (*A_i*) in a chromatogram are proportional to *nF_i*. Separation of products is achieved by gas chromatography (Varian CP-3900) over a non-polar CP-Sil 5 CB (25 m, 0.15 mm ID, 2 μm thickness stationary phase) column and based on mol of C (C-%), as in formulas 1 and 2.

$$X_{n-C_{16}} = \frac{\sum_1^{15} nF_i}{\sum_1^{16} nF_i} \cdot 100 \quad (3)$$

$$S_{C_i} = \frac{\sum_1 nF_i}{\sum_1^{15} nF_i} \cdot 100 \quad (4)$$

The impregnated catalysts were loaded in the reactor as fine powders. The reactor is equipped with a metal grid and felt basket (made by hammering a square piece of grid and felt into the reactor using a 15 mm OD rod) in the isothermal zone. Another basket and stainless steel coiled wire is slid down the tube using a rod with a groove for the wire to close the catalyst zone. This lid can be removed by pulling the

wire. Catalysts are recovered after testing following an overnight drying step under flowing nitrogen. We have opted to use catalyst powders for hydrocracking tests rather than compressed catalyst powder pellets, because zeolite nanosheets have a lower mechanical stability compared to bulk MFI and sacrifice a significant part of their internal mesoporous volume under applied pressure during pelletization.⁴

The hydroconversion of a feedstock into a product boiling at a lower temperature than the boiling point of the original feedstock can be described by pseudo first-order kinetics.⁵ The mass balance equation of an ideal plug flow reactor gives the reactant conversion $X(n-C_{16})$ as a function of space time W/F (kgmol^{-1}) and the first-order apparent rate constant k ($\text{molkg}^{-1}\text{s}^{-1}$) as in [Eq. (5)] or in linear form in [Eq. (6)]. This was demonstrated for heavy gas oil over Pt/BEA and Pt/ Al_2O_3 extrudates⁶ as well as for n-hexadecane over Pt/ SiO_2 - Al_2O_3 powder pellets.⁷

$$X(n - C_{16}) = 1 - e^{-k\frac{W}{F}} \quad (5)$$

$$-\ln(1 - X(n - C_{16})) = k\frac{W}{F} \quad (6)$$

We performed hydrocracking experiments using Pt-1/MFI zeolite powder at various space times with a different amounts of catalyst powder and at varying temperature as shown in Figure S8a. The reaction rate decreases when more than 2 g of catalyst is used, yet the activation energy – derived from the slope of the Arrhenius plot – remains the same. In the event of external diffusion limiting the rate, the activation energy would be no higher than 21 kJmol^{-1} .⁸ Activation energies in this study – in normal hydrocracking in the absence of water – are all around 150 kJmol^{-1} . From Figure S8b it is clear that a strong deviation from ideal plug flow behavior occurs at catalyst powder loadings in excess of 2 g. For this reason, the reaction rates reported in this paper are all obtained with at the most 1 g of catalyst powder, in the absence of external diffusion limitations and with the reactor operated under an ideal plug flow regime.

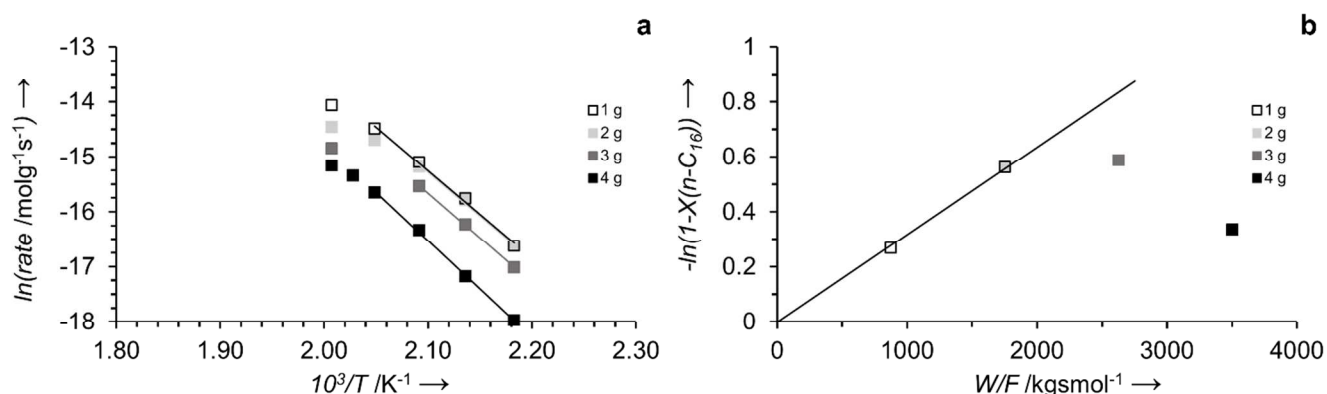


Figure S8. Arrhenius plot of *n*-hexadecane hydrocracking rate (a) over Pt-1/MFI with 0.9 wt.% Pt at W/F : 875 to 3500 kgmol^{-1} with 1 g (\square), 2 g (\blacksquare), 3 g (\blacksquare) and 4 g (\blacksquare) of catalyst powder and from 185 °C to 225 °C, (b) linear fitting to pseudo first order rate equation for ideal plug flow reactor of the data obtained at 205 °C, 20 bar and $\text{H}_2/n\text{-C}_{16} = 10$ mol/mol.

The reactant *n*-hexadecane and water feeds to the reactor were administered with LabAlliance Series 1 HPLC pumps with a lower operating limit of 0.01 ml/min. The feed flow rate range was extended to 0.0025 ml/min with a system of fused silica capillaries of 50 μm ID in order to be able to run hydrocracking experiments at higher space times. Resistance to laminar flow in a capillary is given by the Hagen-Poiseuille equation. The required lengths of the capillaries were calculated from a mass balance of the feed, reactor and vent flows and from the fact that the pressure drop over the vent flow capillary is equal to the combined pressure drop of the capillary to the reactor and of the reactor itself. This is summarized in Table S1 and example flow rates from an actual experiment are given to demonstrate the accuracy.

Table S1. Capillary flow

Hagen-Poiseuille with η : dynamic viscosity of liquid, l : length of capillary, r : radius of capillary		$Q = \frac{\pi r^4 \Delta P}{8 \eta l}$	
Mass balance with Q_{in} : pump flow rate, Q_r : reactor feed flow rate, Q_v : vent flow rate		$Q_{in} = Q_r + Q_v$	
Hydrodynamic pressure head across vent capillary equals pressure head over feed capillary + reactor		$Q_v R_v = Q_r R_r + \Delta P_r$	
Q_{in} pump ^a (ml/min) setpoint / actual	Q_v measured ^a (mlmin^{-1})	Q_r calculated (mlmin^{-1})	$Q_v = \frac{Q_{in} + \frac{\Delta P_r}{R_r}}{1 + \frac{R_v}{R_r}}$
			$Q_r = \frac{Q_{in} - \frac{\Delta P_r}{R_v}}{1 + \frac{R_r}{R_v}}$
0.09 / 0.0863	0.065869	0.02043	
0.05 / 0.0488	0.0385	0.01029	
0.03 / 0.0299	0.0249	0.00502	
0.02 / 0.0202	0.0177	0.00248	

^aThe pump feed flow rate is monitored continuously using a balance, the vent over-flow is collected and weighed to determine flow rates, the reactor feed flow rate is the difference.

The pressure – indicated at the pump – against which the HPLC pump pushed (ΔP) corresponded very well with our calculations. A similar set of capillaries was used to administer H_2O to the reactor, but for

lack of space on the dual tube test installation one pump was used to feed water to two reactors – using four capillaries: one vent over flow capillary and one reactor feed capillary for each of the two reactor tubes.

Yields of isomerization and cracking from n -C₁₆ hydrocracking without and with water

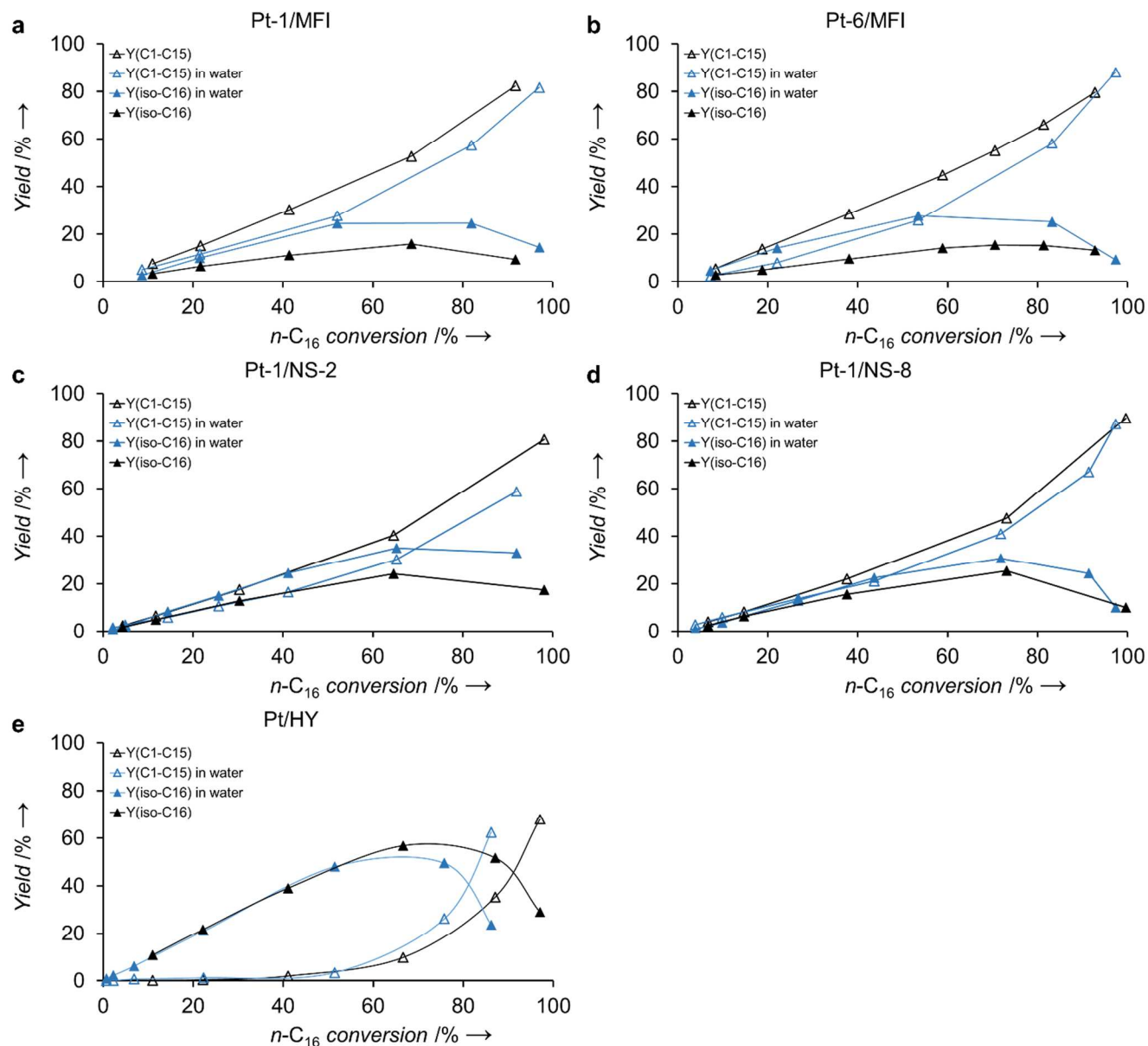


Figure S9. Yields of isomerization: Y(iso-C₁₆) and of cracking products: Y(C₁-C₁₅) against n -C₁₆ conversion in the absence (black) and presence (blue) of H₂O over low heating rate treated Pt-1/MFI (a), high heating rate treated Pt-6/MFI (b), Pt-1/NS-2 (c), Pt-1/NS-8 (d) and Pt/HY (e). Reaction conditions;

20 bar, 1 g of powder, W/F : 875 $\text{kg}\cdot\text{mol}^{-1}$, $\text{H}_2/n\text{-C}_{16}$ molar ratio: 10, $\text{H}_2\text{O}/n\text{-C}_{16}$: 0.8 vol./vol. and temperature ranging from 225 °C to 185 °C (black) and 225 °C to 265 °C (blue) for MFI zeolites and 225 °C to 285 °C for Pt/HY.

Hydrocracking in the presence of water; optimal $\text{H}_2\text{O}/n\text{-C}_{16}$ feed flow ratio

The rate data presented in Figure 2 of the paper were obtained at $\text{H}_2\text{O}/n\text{-C}_{16} = 0.8 \pm 0.1$, which is a compromise between loss of activity and improved selectivity. At a given $n\text{-C}_{16}$ feed flow rate, the reaction rate decreases with increasing water feed flow rate (Figure S10). At 225 °C, the conversion becomes too low to detect any further decrease. Therefore the temperature was increased to 245 °C. The $n\text{-C}_{16}$ reaction rate continues to decrease beyond $\text{H}_2\text{O}/n\text{-C}_{16} = 0.8$ to reach a lower limit at 1.6 from which it no longer decreases with increasing H_2O feed flow rate, in spite of the lower residence time for $n\text{-C}_{16}$. In the presence of water, secondary cracking is minimized with increasing $\text{H}_2\text{O}/n\text{-C}_{16}$ up to a ratio around 0.8 from where only pure primary cracking occurs.

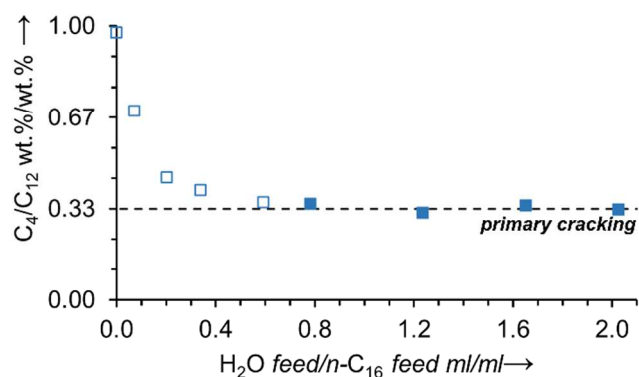


Figure S10. Secondary cracking expressed at C_4/C_{12} weight ratio against H_2O to $n\text{-C}_{16}$ feed flow ratio at 20 bar and 225 °C (□) and 245 °C (■).

Influence of metal loading and metal dispersion on the linearity of the cracking products

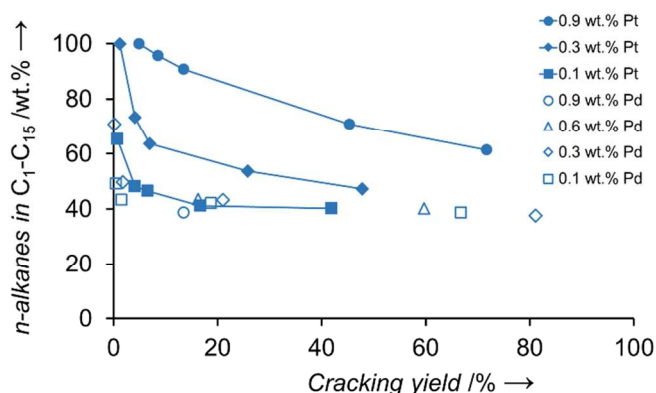


Figure S11. *n*-Alkane percentage of the total cracking products against cracking yield over Pt-1/MFI (full symbols) and Pd/MFI (open symbols) with increasing metal loading from 0.1 wt.% (squares), 0.3 wt.% (diamonds), 0.6 wt.% (triangles) to 0.9 wt.% (circles), at W/F : 875 to 3500 kgsmol^{-1} and between 225 °C – 245 °C.

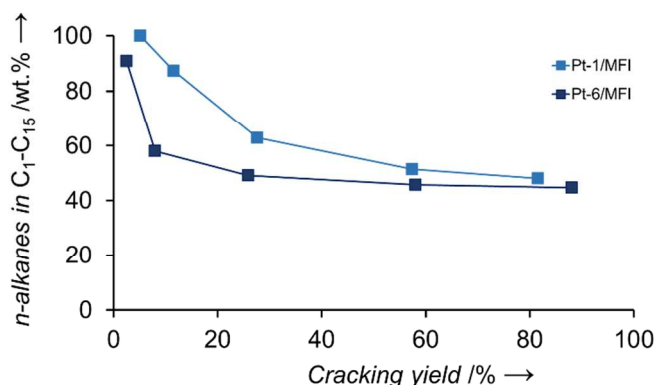


Figure S12. *n*-Alkane percentage of the total cracking products against cracking yield over Pt/MFI after low heating rate, Pt-1/MFI (light blue), and high heating rate Pt-6/MFI (dark blue) at W/F : 875 kgsmol^{-1} and between 225 °C – 265 °C.

Multicomponent flash distillation of the reactor effluent

Multicomponent flash distillations were performed on the overall molar composition (z_i) of the effluent streams F from hydrocracking of $n\text{-C}_{16}$ in the presence of water (a) in between 225 °C and 265 °C – spanning 2 % to 92 % $n\text{-C}_{16}$ conversion – at a space time of 1750 kgsmol^{-1} (LHSV: 0.46 h^{-1}) and (b) at lower temperatures (225 °C – 235 °C) but higher space times of up to 28000 kgsmol^{-1} (LHSV: 0.03 h^{-1}) – spanning 20 % to 95 % $n\text{-C}_{16}$ conversion, over both Pt-1/NS-2 and Pt-1/NS-8 catalysts. The molar compositions z_i are obtained from the product distributions. Molar fractions of H_2O in the liquid phase (x_i) in Figure S13 data set (b), shown in dark blue, are calculated from molar compositions (z_i)

presented in Figure 6 of the manuscript – showing product *n*-alkane (wt.%) versus *n*-C₁₆ conversion (%). The vapor pressures of *n*-C₁₆ cracking products (C₃-C₁₅) were calculated using the Antoine equation and NIST parameters.⁹ Raoult's law [Eq. (7)] was assumed to apply. Substituting into the species balance [Eq. (8)] and summing over all molar compositions in the liquid phase x_i gives [Eq. (9)].

$$y_i = K_i x_i \text{ with } K_i = \frac{P_i^*}{P} \quad (7)$$

$$z_i F = x_i L + y_i V \quad (8)$$

$$L = \sum \frac{z_i F}{1 + K_i \frac{V}{L}} \quad (9)$$

The total liquid molar flow rate L is found by trial and error in an iterative manner. The total liquid molar flow rate L is the sum of the molar liquid flow rates l_i of the individual hydrocarbon products. Their fraction in the liquid x_i and the vapor phase y_i as well as the molar vapor flow rates v_i follow from establishing L . Table S2 documents an example of the effluent stream from hydrocracking over Pt/NS-2 at low and high conversions at low space time and also at low and high conversions at higher space time but lower temperature.

Table S2. H₂O molar fraction in the liquid phase x_i as a function of reaction conditions

X(<i>n</i> -C ₁₆) %	Temperature °C	H ₂ O/ <i>n</i> -C ₁₆	W/F kgmol ⁻¹	z_i mol-%	$x_i = l_i/L$ mol-%	v_i/f_i %
2.12	225	0.79	1693	0.53	0.42	95.2
91.9	265	0.73	1718	0.49	0.21	100.0
21.3	225	0.94	9824	0.58	0.45	95.6
93.3	235	0.92	31378	0.60	0.41	95.7

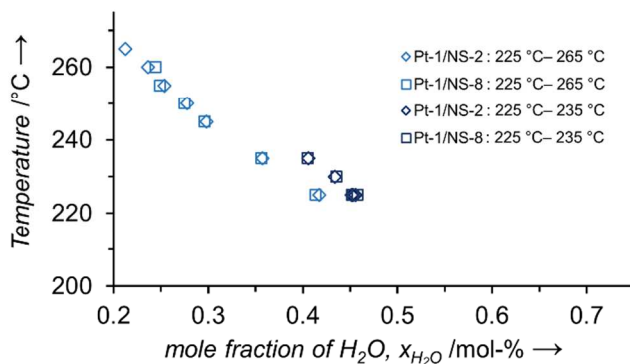


Figure S13. Molar fraction of H₂O in the liquid phase of the trickle bed hydrocracking reactor at 20 bar, H₂O/*n*-C₁₆=0.8 ± 0.1, as determined from flash distillation of the overall composition of the effluent

product stream from hydrocracking over Pt-1/NS-2 and Pt-1/NS-8: temperature range (a) 225–265 °C (light blue), (b) 225–235 °C (dark blue).

References

- [1] Choi, M.; Na, K.; Kim, J.; Sakamoto, Y.; Terasaki, O.; Ryoo, R. *Nature* **2009**, 461, 246-250.
- [2] Machoke, A. G.; Knoke, I. Y.; Lopez-Orozco, S.; Schmiele, M.; Selvam, T.; Marthala, V. R. R.; Spiecker, E.; Unruh, T.; Hartmann, M.; Schwieger, W. *Micro. Meso. Mat.* **2014**, 190, 324-333.
- [3] Jo, C.; Cho, K.; Kim, J.; Ryoo, R. *Chem. Commun.* **2014**, 50, 4175-4177.
- [4] Na, K.; Park, W.; Seo, Y.; Ryoo, R. *Chem. Mater.* **2011**, 23, 1273-1279.
- [5] Krishna, R. *Erdoel, Kohle, Erdgas, Petrochem. Brennst. Chem.* **1989**, 42, 194-199.
- [6] Landau, M. V.; Vradman, L.; Valtchev, V.; Lezervant, J.; Liubich, E.; Talianker, M. *Ind. Eng. Chem. Res.* **2003**, 42, 2773-2782.
- [7] Regali, F.; Boutonnet, M.; Järås, S. *Catal. Today* **2013**, 214, 12-18.
- [8] Le Page, A. J. F. *Applied heterogeneous catalysis*, Gulf Publishing Company, Houston, **1988**, p. 49.
- [9] Linstrom, P. J.; Mallard, W. G., Eds. *NIST Chemistry WebBook, NIST standard reference database No. 69*, National Institute of Standards and Technology, Gaithersburg MD, 20899, <http://webbook.nist.gov>, (retrieved May 31, 2016).